Tuning of PCDTBT:PC71BM blend nanoparticles for eco-friendly processing of polymer solar cells

Peer-reviewed author version

D'OLIESLAEGER, Lien; Pfannmoller, Martin; Fron, Eduard; CARDINALETTI, Ilaria; Van der Auweraer, Mark; Van Tendeloo, Gustaaf; Bals, Sara; MAES, Wouter; VANDERZANDE, Dirk; MANCA, Jean & ETHIRAJAN, Anitha (2017) Tuning of PCDTBT:PC71BM blend nanoparticles for eco-friendly processing of polymer solar cells. In: SOLAR ENERGY MATERIALS AND SOLAR CELLS, 159, p. 179-188.

DOI: 10.1016/j.solmat.2016.09.008
Handle: http://hdl.handle.net/1942/23033

Tuning of PCDTBT:$PC_{71}BM$ blend nanoparticles for eco-friendly processing of polymer solar cells

Lien D'Olieslaeger,[a] Martin Pfannmöller,[b] Eduard Fron,[c] Ilaria Cardinaletti,[a] Mark Van Der Auweraer,[c] Gustaaf Van Tendeloo, [b] Sara Bals,[b] Wouter Maes,[a,d] Dirk Vanderzande,[a,d] Jean Manca,[e] and Anitha Ethirajan[a,d*]

[a] Institute for Materials Research (IMO-IMOMEC), Hasselt university, Wetenschapspark 1 and Agoralaan 1 - Building D, B-3590 Diepenbeek, Belgium

[b] EMAT, Antwerp University, Groenenborgerlaan 171, B-2020 Antwerp, Belgium

[c] KU Leuven, Department of Chemistry, Division of Molecular Imaging and Photonics, Celestijnenlaan 200F, B-3001 Heverlee, Belgium

[d] IMEC, Associated lab IMOMEC, Wetenschapspark 1, 3590 Diepenbeek, Belgium

[e] X-LaB, Hasselt University, Agoralaan 1 - Building D, B-3590 Diepenbeek, Belgium

ABSTRACT

We report the controlled preparation of water processable nanoparticles (NPs) employing the push-pull polymer PCDTBT and the fullerene acceptor $PC_{71}BM$ in order to enable solar cell processing using eco-friendly solvent (i.e. water). The presented method provides the possibility to separate the formation of the active layer blend and the deposition of the active layer into two different processes. For the first time, the benefits of aqueous processability for the high-potential class of push-pull polymers, generally requiring high boiling solvents, are made accessible. With our method we demonstrate excellent control over the blend stoichiometry and efficient mixing. Furthermore, we provide visualization of the nanomorphology of the different NPs to obtain structural information down to ~2 nm resolution using advanced analytical electron microscopy. The imaging directly reveals very small compositional demixing in the PCDTBT:$PC_{71}BM$ blend NPs, in the size range of about <5 nm, indicating fine mixing at the molecular level. The suitability of the proposed methodology and materials towards the aspects of eco-friendly processing of organic solar cells is demonstrated through a processing of lab scale NPs solar cell prototypes reaching a power conversion efficiency of 1.9%.

KEYWORDS

PCDTBT:$PC_{71}BM$ blend nanoparticles, nanomorphology, time-resolved fluorescence spectroscopy, STEMSI, eco-friendly, solar cells

1. INTRODUCTION

Bulk heterojunction (BHJ) organic photovoltaics have obtained a tremendous interest over the years because of some highly desirable properties such as mechanical flexibility, (semi)transparency, low cost and printability [1,2,3,4]. As the energy gap of the absorber is decisive for converting light into electricity, remarkable progress in the material design has led to the development of materials capable of efficiently harvesting solar light. In this regard, donor-acceptor or push-pull type low bandgap polymers, consisting of alternating electron-rich and

electron-deficient moieties along the conjugated polymer backbone, enabled significant advances in terms of power conversion efficiencies (PCEs) [5,6]. Because of the rapid development in the synthetic methodologies, a plethora of push-pull polymers - PCDTBT (poly{[9-(1'-octylnonyl)-9*H*-carbazole-2,7-diyl]-2,5-thiophenediyl-2,1,3-benzothiadiazole-4,7-diyl-2,5-thiophene-diyl}), PBDTTPD (poly{di(2'-ethylhexyloxy)benzo[1,2-*b*:4,5-*b*']dithiophene-*co*-octylthieno[3,4-*c*]pyrrole-4,6-dione}) and PffBT4T-2OD (poly[(5,6-difluoro-2,1,3-benzothiadiazol-4,7-diyl)-*alt*-(3,3'''-di(2-octyldodecyl)-2,2';5',2'';5'',2'''-quaterthiophen-5,5'''-diyl)]) to name a few - excelling the performance of previous generation materials, are now available and still emerging [6,7,8,9,10,11,12].

As the BHJ photoactive layer can be processed from solution, different deposition techniques related to printing and coating are easily accessible, such as screen printing, inkjet printing, spray coating and slot-die coating [13]. However, the use of hazardous solvents for fabrication is contentious and has raised serious concerns on this 'green energy' technology owing to the associated impact on the environment. Therefore, transfer of BHJ OPV technology from the lab-scale to large-scale fabrication is still hindered. Many reports already exists on the green solvent processability of polymer solar cells [14,15,16]. Another promising alternative for ecofriendly fabrication of organic solar cells would be water-based dispersions of polymer nanoparticles (NPs) comprising the active layer blend materials, as they provide the possibility to separate the formation of the active layer blend and the deposition of the active layer into two different processes. This eliminates the use of hazardous organic solvents in large amounts during the large-scale fabrication of solar cells, thereby easing the hurdles in manufacturing with respect to health, environment and handling safety. Also, during the particle formation process, the solvent evaporation step can in principle be made into a closed loop process, thereby allowing the recycling of the solvent in a controlled way. Moreover, the amount of solvent needed for preparing the nanoparticle dispersion is relatively small as compared to the solvent amount used for deposition of the active layer (using different coating techniques) depending upon viscosity requirements[17]. As a result, the use of aqueous dispersions of conjugated polymer NPs for eco-friendly device fabrication has generated a great deal of interest. Several research groups have reported OPVs processed from aqueous dispersions of NPs generated by reprecipitation or by miniemulsion techniques [18,18,19,20,21,22,23,24,25,26,27,28,29,30,31,32,33]. Both techniques, however, rely on good solubility of the polymers in the chosen organic solvent. Moreover, the used procedure necessitates the use of low boiling solvents such as chloroform (bp = 61 °C, vp = 160 mmHg) and especially only solvents that are miscible with water, such as THF (bp = 66 °C, vp = 132 mmHg), in case of the reprecipitation method. So far, only a limited choice of push-pull materials were tested and this was restricted mostly to materials in the molecular weight range of 6 kDa<M_n<40 kDa (due to solubility difficulties at high molecular weights) [22,24,32,33]. Recently, a particular DPP-based push-pull polymer with a M_n of 53 kDa was formed into particles. However, in the latter case the material was soluble in chloroform [30]. These stringent conditions make the aqueous processability inaccessible for the highly interesting polymers that are not soluble in the low boiling solvents currently in use. Therefore, particle generation methodologies that allow for the generation of donor-acceptor blend NPs with well-defined stoichiometry are highly desired for push-pull polymers.

Among the OPV-type push-pull polymers, PCDTBT is an established material with several existing studies related to device characteristics, optoelectronic properties and morphology of BHJ films [34,35,36,37,38,39,40,41,42]. With high photochemical stability, the devices have been shown to possess excellent operational lifetime, both under laboratory and real-world conditions [3,4,8]. Previously, depending on the molecular weight, chloroform, chlorobenzene, *o*-dichlorobenzene (*o*-DCB), trichlorobenzene, and several mixtures of solvents were used to process PCDTBT:$PC_{71}BM$([6,6]-Phenyl-C_{71}-butyric acid methyl ester) devices [36,38,41]. It was shown that with increasing molecular weight, the low boiling solvents could not be used anymore. *o*-DCB has been reported as an optimal solvent for achieving high power conversion efficiencies (PCEs) in the case of PCDTBT:$PC_{71}BM$ blend BHJ devices [39]. As with high molecular weight the solubility in low boiling point solvents becomes a limiting factor

[7], the formulation of NPs is not feasible. In addition, the need to use higher molecular weight polymers for better device performance [7,43,44] codetermines the stringency of particle formation.

To overcome the above-mentioned challenges, we present a pioneering particle formulation procedure that allows the use of a high boiling solvent, *o*-DCB, to obtain water-based push-pull polymer:fullerene (PCDTBT:$PC_{71}BM$) blend NPs, thereby extending the benefit of aqueous processability to the highly interesting class of push-pull polymers requiring high boiling solvents. Our method brings the previously reported miniemulsion technique a significant step further [29,45]. We demonstrate excellent control over the stoichiometry, despite using the combination of a high boiling solvent and high molecular weight polymer (see Figure 1). The former can impede the colloidal stability as well as affect the size distribution [46] during evaporation, whereas the latter can influence the particle formation due to increased viscosity and consequently affect the homogeneous blending with the acceptor molecules. The blend morphology with a systematic variation of the blend stoichiometries was attained by slow evaporation of the solvent using temperatures (60 °C) well below the glass transition temperature (130 °C [47]) of the polymer. The optical properties of the particles of different blend compositions were studied using optical spectroscopy techniques. To accompany the bulk measurements, the morphology of different NPs was investigated using advanced characterization by spectroscopic imaging in analytical scanning transmission electron microscopy (STEM). Among the many methods that have been applied in reciprocal and real space [48], TEM has been shown to be able to obtain information at the nanoscale, and create chemical contrast between two very similar materials using analytical TEM modalities [49]. So far, to the best of our knowledge, morphological characterization of blend NPs was done mainly with scanning transmission X-ray microscopy (STXM) [19,22,23]. STXM provides superior chemical contrast between different polymers or polymers and fullerenes, but is limited by its resolution of ~30 nm, which was enhanced by post processing to ~10 nm by assuming certain possible models of the morphology [20].

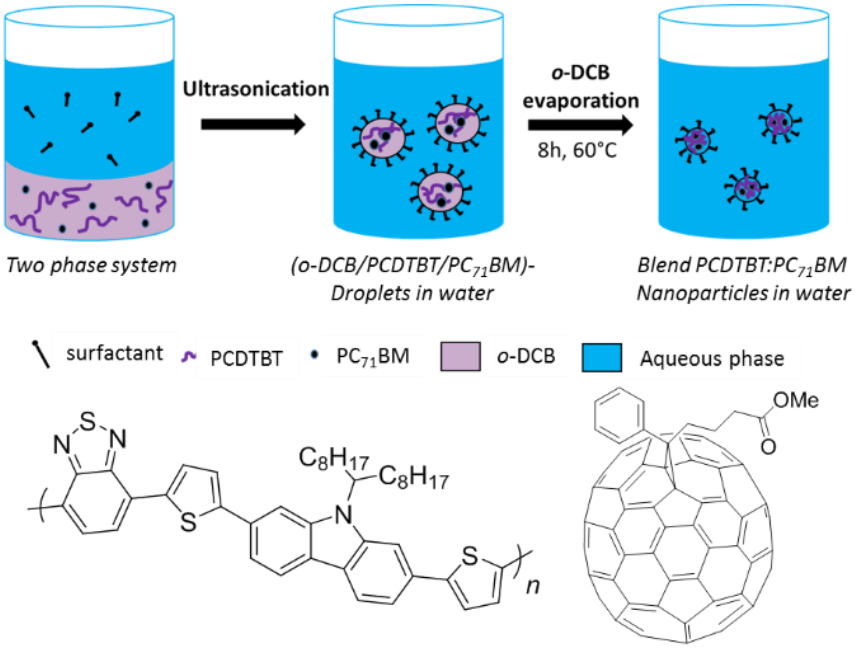

Figure 1. (Top) Schematic illustration of the PCDTBT:$PC_{71}BM$ blend NP synthesis. **(Bottom)** Chemical structures of PCDTBT **(Left)** and $PC_{71}BM$ **(Right)**.

It has been previously shown that PCDTBT:$PC_{71}BM$ undergoes efficient mixing [34]. As indicated before, with higher molecular weights, the solubility of PCDTBT decreases. Often, the polymer solutions in $CHCl_3$ or *o*-DCB are passed through filters to eliminate undissolved aggregates and then further used for film formation. Considering

the limited solubility of the polymer, during the blend particle formation process, increased local concentrations due to evaporation of the solvent might result in phase separation heterogeneities within the blend structure. Therefore, in this article, analytical electron microscopy was applied to obtain structural information down to ~2 nm resolution by employing scanning transmission electron microscopy (STEM) in combination with electron energy-loss spectroscopy, which is referred to as STEM spectral imaging (STEMSI). Finally, as a proof of concept, an eco-friendly OPV device was prepared using the water-based blend NPs. The active layer nanomorphology in the device structure was studied and correlated to the one observed within the nanoparticles.

2. EXPERIMENTAL

2.1 Materials

Poly{[9-(1'-octylnonyl)-9*H*-carbazole-2,7-diyl]-2,5-thiophene-diyl-2,1,3-benzothiadiazole-4,7-diyl-2,5-thiophene-diyl} (PCDTBT) was obtained from SolarisChem (M_n = 79 kDa, $Đ$ = 2.4) and used without further purification. [6,6]-Phenyl-C_{71}-butyric acid methyl ester ($PC_{71}BM$) (purity >99%) was obtained from Solenne. *o*-Dichlorobenzene (purity >99%) was obtained from Sigma Aldrich and sodium dodecyl sulfate (SDS) from Merck. Zinc oxide (ZnO) nanoparticles were obtained from nanograde, indium thin oxide (ITO) glass slides (20 Ω sq^{-1}) from Kintec.

2.2 Synthesis of blend nanoparticles

Different ratios of the donor polymer and the fullerene acceptor were dissolved in 2 g *o*-DCB at elevated temperature (as the polymer was not soluble at room temperature). The ratio of the active material to the solvent was optimized to ensure complete solubility of the ingredients, where visibly no aggregates could be seen. It is worth to note that there were batch-to-batch variations in the polymer of the same molecular weight range, as the solubility in the solvent varied. The conditions provided here were optimized after several trial-and-error tests using the same batch of polymer, different concentration ranges and temperature conditions. The polymer was dissolved by magnetic stirring (500 revolutions per minute, rpm) at 80 °C in a nitrogen environment. As the amount of solvent in the dispersed phase is higher than the usual procedures reported for miniemulsion/solvent evaporation, the ratio between the dispersed phase and the continuous phase was optimized to obtain stable dispersions with reasonable solid content. For the miniemulsion formulation, at first, a macro-emulsion was obtained by adding the aqueous phase, consisting of 11 mg dissolved surfactant (SDS) in 2.64 g water (0.4 wt%), to the organic phase. After magnetic stirring of the mixture for one hour, the macro-emulsion was subjected to ultrasonication under ice cooling for 3 min at 60% amplitude in a pulse regime (30 s pulse, 20 s pause) using a Branson 450W digital sonifier (1/8" tip). The obtained miniemulsion was transferred into a round bottom flask with a wide neck and left for 8 h at 60 °C to allow complete evaporation of the organic solvent. Every hour, additional water was added to the miniemulsion to compensate for the water lost during evaporation and to avoid altering the SDS to water concentration ratio in the continuous phase. Excess surfactant was removed by multiple washing steps using Millipore membrane tubes (MWCO: 30 kDa).

2.3 Dynamic light scattering (DLS)

The size and size distribution of all NPs was characterized by DLS using a Brookhaven Instruments Zetapals.

2.4 Optical analysis

The UV-Vis absorption spectra of the NPs were measured using an Agilent Cary500 Scan UV-Vis-NIR spectrophotometer and a Lambda 40, Perkin Elmer UV-VIS spectrophotometer. All NP samples were measured at

a fixed solid content of 0.0018 wt%. The emission spectra of the PCDTBT:$PC_{71}BM$ blend nanoparticles were obtained using a Horiba-Jobin Yvon FluoroLog-3 spectrofluorometer which was corrected for the wavelength dependence of the throughput and sensitivity of the detection channel. A quantum counter was used to correct for temporal fluctuations in the excitation intensity as well for the wavelength dependence of the excitation intensity.

2.5 Time-resolved fluorescence decay experiments

On a nano- and picoseconds timescale, the fluorescence decays were obtained by Time-Correlated Single Photon Counting (TCSPC), described in detail previously [50]. A time-correlated Single Photon Timing PC module (SPC 830, Becker & Hickl) was used to obtain the fluorescence decay histogram in 4,096 channels. The decays were recorded with 10,000 counts in the peak channel, in time windows of 6 ns corresponding to 1.46 ps/channel, and analysed globally by linking the decay times of decays obtained at different wavelengths as a sum of exponentials, with the time-resolved fluorescence analysis (TRFA) software [40]. The time resolution of this set-up is about 30 to 50 ps. All NP samples were measured at a fixed solid content of 0.0002 Wt%.

2.6 Scanning transmission electron microscopy

To prepare samples for electron microscopic analysis, 3 µL of the NP dispersion was dropcasted onto plasma cleaned grids with holey carbon films (Quantifoil). Most of the liquid was removed by filter paper after 1 min. A subset of single particles or agglomerates can be found at the edges of the Quantifoil holes. This allows imaging with vacuum background. Before STEMSI investigations, the particles were also examined with conventional bright-field TEM. TEM analysis was done using an FEI Tecnai G2 microscope at an acceleration voltage of 200 kV. Dark-field STEM and STEMSI was performed with an FEI Titan G3 microscope at an acceleration voltage of 120 kV. Acquisition of the spectroscopic data is enabled by a GIF Enfinium dedicated spectrometer (Gatan). The energy dispersion was chosen to be 0.05 eV/channel, offering a sufficient oversampling regarding the instrumental energy resolution without monochromated settings of ~0.7 eV. The electron dose to acquire low energy-loss spectra up to ~90 eV was approximately 1200 e/A^2 for the pure samples, using a STEM step size of 2 nm, and 2700 e/A^2 for the blend sample, using a step size of 1.3 nm. This dose was shown to not significantly alter the bulk plasmon peak positions for P3HT and $PC_{61}BM$ [51].

For plasmon peak fitting, the STEMSI data sets were deconvoluted applying Fourier-Log deconvolution [52]. Due to the thickness of the NPs, a distribution of single-scattering, double or multi-scattering can be observed. This induces varying intensities on the sides of the plasmon peaks depending on the actual thickness. With deconvolution single scattering distributions can be obtained [53], which allows better comparison of the spectra between different particles. Plasmon peaks were fitted with a Lorentzian profile to determine the central positions, which are mapped out to obtain morphological images. For average spectra of the different samples, areas from the insides of the particles (avoiding perimeters) were selected, followed by averaging and normalization to identical integrals, i.e. areas below the curves. This compensates for global intensity differences between data sets of different samples. The cross-section of the solar cell device was prepared by focused ion beam milling using a Helios NanoLab 650 (FEI) to a thickness of ca. 60 nm. The final thinning of the cross-section was performed with an acceleration voltage of 2 kV to prevent damaging the organic materials by high-energy ions. Dark-field and STEMSI was applied as for the NPs. However, the resulting plasmon peak map was smoothed by a Gaussian filter (size 3x3) to illustrate occasions of minor demixing.

2.7 Device fabrication

Solar cells were fabricated on pre-cleaned patterned ITO glass slides which were cleaned with detergent, water, acetone and boiling isopropanol. Afterwards the substrates were treated with UV-ozone for 30 minutes. A ZnO

nanoparticles layer was spincoated (0.1 wt% in isopropanol, 4000 rpm) and annealed at 150 °C for 10 minutes in a nitrogen atmosphere. Then, the PCDTBT:$PC_{71}BM$ (400 wt%; 1:4) nanoparticle layers were deposited by spincoating the dispersion (300 µL, 4% solid content, 2000 rpm). A 1:4 PCDTBT:$PC_{71}BM$ ratio in the particle was chosen in analogy to the conventional (optimized) BHJ device ratio [54]. The thickness of the spincoated layer was 100 nm, as measured by a DektakXT stylus profiler from Bruker. Afterwards, the substrates were heated for 4 min at 180 °C (and also at other temperatures (supporting information)) in a nitrogen atmosphere for film formation and to eliminate residual water. The film was then transferred into a vacuum chamber for electrode evaporation. MoO_3/Al electrodes were evaporated on top of the active layer, resulting in an active area of 0.3 cm^2. The thickness of the MoO_3 and Al electrodes were measured to be 20 and 120 nm, respectively, using a quartz crystal monitor.

2.8 Atomic Force Microscopy

The NP layer coverage, before and after annealing, was imaged in tapping mode using a Bruker Multimode 8 atomic force microscope.

3. RESULTS & DISCUSSION

3.1 Blend nanoparticle synthesis

PCDTBT:$PC_{71}BM$ blend nanoparticles were synthesized combining the miniemulsion and the emulsion solvent evaporation techniques. PCDTBT is a polymer that shows solubility issues and is therefore not soluble in any of the low boiling point solvents. As *o*-DCB has been reported as an optimal solvent for achieving high PCEs in the case of PCDTBT:$PC_{71}BM$ blends, it was used as the solvent for fabrication of the blend NPs by adapting the procedure previously developed by Landfester et al. [55], where only low boiling point solvents were used so far. The evaporation of *o*-DCB was performed at 60 °C and the inevitable loss of water during the prolonged evaporation was compensated by the incorporation of water to the continuous phase at regular intervals. The obtained colloidally stable dispersions were characterized for their size by DLS. A crucial factor underpinning the device performance is the complex interplay between the blend morphology in the solid state and the resulting optoelectronic properties. The optical properties of the particles were characterized using different variants of optical spectroscopic techniques and the nanomorphology was studied at the single nanoparticle level by STEMSI. Using the synthesis procedure, as depicted in Figure 1, PCDTBT:$PC_{71}BM$ NPs of various blend compositions were prepared and subsequently washed to remove the surfactant. As can be seen in Table 1, the average particle size for the blend NPs lies between 36 and 74 nm. Although there is no characteristic variation in size as a function of $PC_{71}BM$ incorporation, it can be expected that the dimensions of the different NPs might vary depending on the compactness of the particles as a result of the composition (large molecular weight PCDTBT chains and small molecular weight $PC_{71}BM$) used for particle formation. The polydispersity index (PDI), describing the distribution width, of all synthesized particles is included in Table 1. The observed polydispersity, ranging from 0.104 to 0.216, can be attributed to the inherent characteristics of the particle formation process, as was shown by Staff et al [46]. It is expected that the dimensions of the different NPs vary depending on the compactness of the particles as a result of the composition (large molecular weight PCDTBT chains and small molecular weight $PC_{71}BM$) used. The solid content of the particle dispersions is in the expected range between 0.2 and 0.4% as water was added during the synthesis.

Table 1. Characterization of the blend PCDTBT:$PC_{71}BM$ nanoparticles with varying ratios of PCDTBT/$PC_{71}BM$.

Sample	PCDTBT (mg)	$PC_{71}BM^{a}$ (%)	Size (nm)	PDI
NP1-0% $PC_{71}BM$	25	0	61	0.145
NP2-1% $PC_{71}BM$	25	1	52	0.175
NP3-2.5% $PC_{71}BM$	25	2.5	74	0.104
NP4-5% $PC_{71}BM$	25	5	50	0.253
NP5-25% $PC_{71}BM$	25	25	55	0.177
NP6-50% $PC_{71}BM$	25	50	52	0.187
NP7-75% $PC_{71}BM$	25	75	48	0.216
NP8-100% $PC_{71}BM$	0	100	36	0.144

[a] *Weight percentage with respect to the amount of PCDTBT.*

3.2 Optical properties of the blend nanoparticles

As the optoelectronic properties of the blend NPs are morphology dependent, the study of their optical properties can provide insights into the efficiency of mixing and aggregation behavior of the particle constituents. The optical properties of aqueous dispersions of the NPs with controlled variations in stoichiometry were systematically studied using UV-Vis absorption and emission as well as time-resolved fluorescence spectroscopy (Figure 2). Similar studies have been previously reported for P3HT:$PC_{61}BM$, MEH-PPV:$PC_{61}BM$ NPs [26,27,28,56] and PCDTBT:$PC_{71}BM$ films [41]. It can be seen in Figure 2A that for pure PCDTBT nanoparticles the UV-Vis spectra are characterized by an $S_0 \rightarrow S_1$ band around 540 nm, which can be attributed to an intramolecular charge transfer state transition, and an $S_0 \rightarrow S_2$ band around 380 nm. The fluorescence emission maximum is located at 702 nm, which is in agreement to the maximum observed for films in literature [36]. The UV-Vis absorption spectra of PCDTBT:$PC_{71}BM$ blends of different blend ratios in the form of NPs and molecularly dissolved in *o*-DCB are presented in Figure S1 (supporting information).

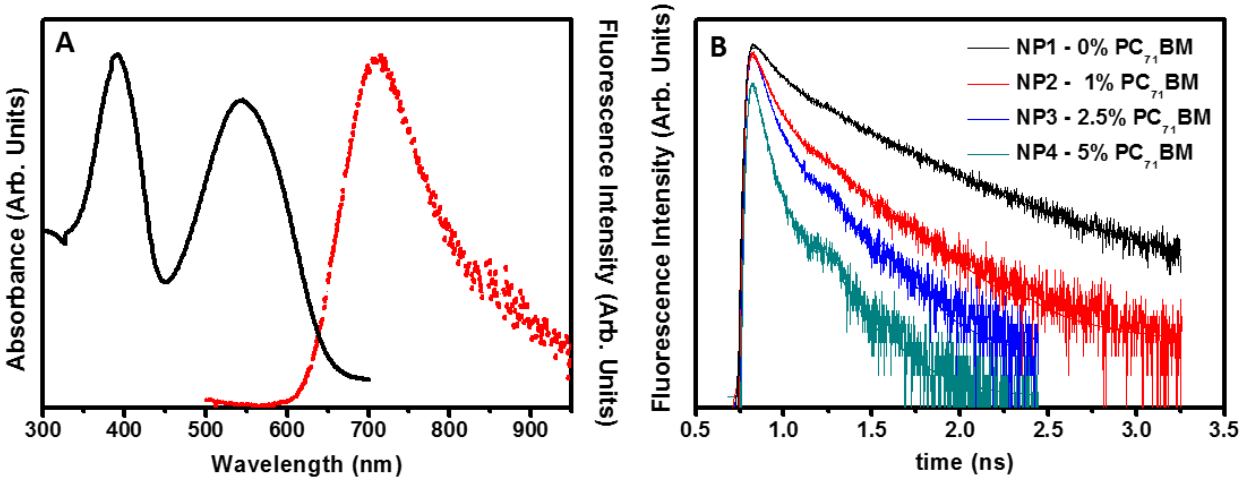

Figure 2. (A) UV-Vis absorption spectrum (black) and fluorescence emission spectrum (red) of pure PCDTBT NPs (NP1-0% $PC_{71}BM$). **(B)** Fluorescence decays obtained by single photon timing (λ_{ex} = 550 nm; λ_{em} = 670 nm) of PCDTBT:$PC_{71}BM$ blend NPs in water.

The fluorescence decays of the PCDTBT:$PC_{71}BM$ blend NPs, depicted in Figure 2B, could for all samples be analyzed as a sum of two exponentials (equation 1) yielding two components with positive amplitude (α_1 and α_2).

$$I(t) = \sum \alpha_i e^{-t/\tau_i i} \qquad \text{Eq. 1}$$

The decay times (τ_i) and corresponding amplitudes (α_i), where the sum of the positive amplitudes is normalized to 1, are presented in Table 2. The two decay times, however, can be used to calculate an average decay time $< \tau >$ of the fluorescence of PCDTBT according to equation 2.

$$< \tau >= \sum \alpha_i \tau_i \qquad \text{Eq. 2}$$

Table 2. Decay times (τ_i) and corresponding amplitudes (α_i) obtained by analyzing the fluorescence decays at 670 nm obtained by TCSPC. Excitation occurred at 550 nm. The sum of the α_i was normalized to one.

Sample	τ_1 (ps)/ α_1	τ_2 (ps)/ α_2	$< \tau >$ (ps)
NP1-0% $PC_{71}BM$	90 / 0.67	478 / 0.33	218
NP2-1% $PC_{71}BM$	62 / 0.85	312 / 0.15	100
NP3-2.5% $PC_{71}BM$	42 / 0.87	180 / 0.13	60
NP4-5% $PC_{71}BM$	34 / 0.96	207 / 0.04	41
F1-0% $PC_{71}BM$	75 / 0.73	444 / 0.27	175

Interestingly, the decay times measured for a neat polymer film (F1) were similar to those obtained for the neat polymer particles (NP1-0% $PC_{71}BM$), thereby reflecting the similarity in the aggregation behavior of the polymer in the films and in NPs. For the NPs of neat PCDTBT (NP1-0% $PC_{71}BM$), the decay times are close to the two longest decay times observed by Banerji et al. for a film of PCDTBT, where the fluorescence was analyzed as a sum of four exponentials [36]. As the carrier generation efficiency is independent of the excitation wavelength, the measurements were not repeated for excitation at 400 nm.[38] Both decay times decrease upon increasing the concentration of $PC_{71}BM$, while the amplitude of the fast decaying component increases upon increasing the concentration of $PC_{71}BM$. At a concentration of 2.5 Wt% $PC_{71}BM$, the shortest decay time is already close to or beyond the time resolution of the employed set-up and the value of $< \tau >$ can be overestimated. Regardless, already at a loading of 1 Wt% $PC_{71}BM$ a major decrease of $< \tau >$ is observed for the NPs. Further increasing the loading of $PC_{71}BM$ leads to a further systematic decrease of $< \tau >$. This trend in the average fluorescence decay time is also followed up to a loading of 25% $PC_{71}BM$ when fluorescence quantum yields are recorded (see Table S1, supporting information). This indicates an effective quenching of the excited PCDTBT by $PC_{71}BM$ in the NPs. The decay trend also clearly confirms that the stoichiometry of the NPs can be controlled in a very systematic way during the synthesis.

3.3 Morphology of the blend nanoparticles

For the nanoscale morphological analysis, three different samples (NP1-0% $PC_{71}BM$, NP7-75% $PC_{71}BM$, NP8-100% $PC_{71}BM$; see Table 1) reflecting the characteristics of the materials (neat and blend composition) were first studied using conventional bright-field TEM. Figure 3A and B shows micrographs of pure PCDTBT and $PC_{71}BM$ nanoparticles, respectively. In both images, homogeneous intensities throughout the particles are observed, with a gradient towards the particle-vacuum interface, where the thickness decreases. In Figure 3C, a collection of blend particles with 75 Wt% $PC_{71}BM$ is presented. The homogeneous intensity distribution for the blend material

shows no internal contrast patterns that could indicate a phase separation. Sizes range from approximately 30 to 70 nm, which is in agreement with the size distribution determined using DLS. Independent of the size, no structure is seen within the particles. The intensity gradients look very similar to that of the pure particles (see defocus series in Figure S2, supporting information).

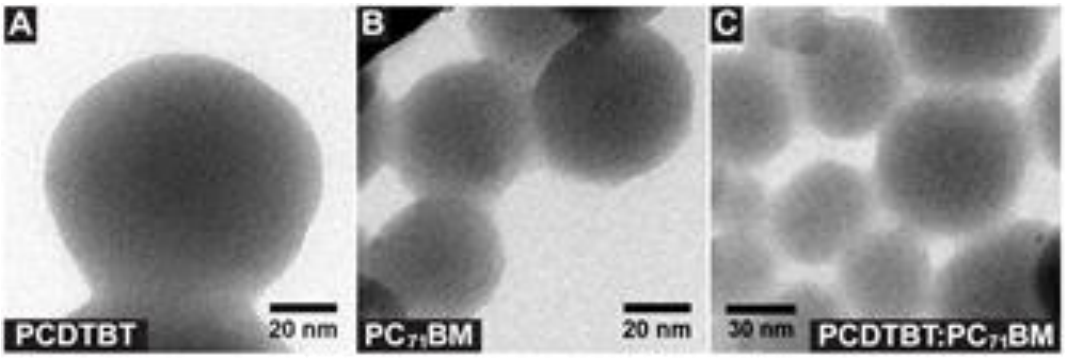

Figure 3. Bright-field TEM images of pure PCDTBT particles **(A)** (NP1-0% $PC_{71}BM$), pure $PC_{71}BM$ particles **(B)** (NP8-100% $PC_{71}BM$) and blend NPs **(C)** (NP7-75% $PC_{71}BM$).

As bright-field TEM has been proven to be unsuitable for the visualization of domains of small compositional differences [49], we applied STEMSI to identify distinct spectral properties that would reveal a possible phase separation within the particles. It was shown before that low energy-loss spectra with information about optical excitations can be used to distinguish different phases, i.e. polymer-enriched, fullerene-enriched as well as mixed phases [57,58,59,60]. This is due to the fact that different carbonaceous materials show different excitations of valence electrons, which can either be bandgap, surface plasmon or bulk plasmon excitations. Since irradiation with electrons causes rapid damage of the materials, the electronic structure determining the bandgap is difficult to probe on the local scale. However, bulk plasmon excitations between ~20-25 eV are much more stable, indicating that the damaged products of polymer chains and fullerene molecules still show a different structure and can hence be distinguished [51,61,62]. Therefore, the spectra of NPs of different compositions is anticipated to show the expected variations. The samples depicted in Figure 3 were further investigated and the results are presented in Figure 4.

By fitting the bulk plasmon peak energy for each scan position of the STEMSI data sets, nanoscale morphological maps of single particles are obtained. Dark-field STEM images of the three investigated samples are provided in Figure 4 A-C. Here, intensities are highly dependent on the thickness of the particles. It is, however, not expected that different domains of slightly different composition can be revealed, due to the rapid radiation damage that can alter density differences [51]. Figure 4 D-E shows dark-field overlays, with maps of plasmon peak positions provided in Figure 4 G-H, for pure PCDTBT and pure $PC_{71}BM$ particles. It can be seen that there is a difference in plasmon peak positions to an amount of almost 2.5 eV, with ~24.8 eV for $PC_{71}BM$ and ~22.4 eV for PCDTBT. As mentioned earlier, such a property of an optical excitation allows separation of enriched and mixed domains in blend systems. The plasmon map (Figure 4I) overlay with the dark-field image for the blend particles is shown in Figure 4F. Values are well in between the extreme values for the pure materials, which indicates that both materials are present, as expected. The plasmon peak energy is almost identical throughout the inside of the particles. In Figure 4J, average spectra of the inner areas from particles of the three samples are shown. Spectra were deconvolved by Fourier-log deconvolution and normalized revealing the differences in several optical excitations. The plasmon peak positions are indicated by lines. In addition, differences in other optical features like π-plasmon excitations around 6 eV can be observed, which implies that the applied electron dose was small

enough to retain important characteristic differences of the electronic structures. Therefore we can also be certain that sufficient differences in bulk plasmon excitations were preserved to visualize a possible nanoscale phase separation. It was shown in several works that domains within polymer:fullerene blends can be reliably visualized using these signals, even after considerable electron irradiation [57,58,61,63]. Moreover, morphology was not affected when comparing results from spectroscopic imaging after corrected TEM imaging on the identical area [49].

Consequently, mapping of the plasmon peaks by low energy-loss STEMSI revealed that the blend particles show no phase separation. By the implication of using projection data of the three-dimensional particles, it is possible that a fine, overlapping separation occurs. The diameters of the investigated particles are in the range of 30-70 nm. It was shown previously that even a phase separation of only several nanometers can be identified within BHJ layers having such a thickness [57]. Hence, although with bright-field TEM and dark-field STEM it might not be possible to visualize it, fine spectroscopic differences would be seen by the spatial spectroscopic mapping. From the maps it can also be inferred that there is no polymer shell around an enriched $PC_{71}BM$ core as observed for P3HT:$PC_{61}BM$ [23] and PFB:F8BT polymer-only particles [20]. A gradient of decreasing plasmon peak energies towards the particle-vacuum interfaces is observed. For the particles depicted in Figure 4F, the decrease in energy from approximately 23.3 to 23.1 eV is detected at a distance of ~4 nm from the interface. In case of a PCDTBT shell, a decrease towards the value measured for pure polymer particles would be expected at this position. The observed decrease, reaching even smaller values directly at the interface and beyond, are due to surface plasmon excitations, which are found approximately at the energy of the bulk plasmon energy divided by √2 [52]. Due to the delocalization of this excitation, a certain contribution is already seen within the particle near the interfaces. Lack of resolution as a cause for not visualizing a polymer shell can also be ruled out. In Figure 4I, the white arrow points to a small area where parts of the outer areas of two particles are joined. Here, a structure can be seen with the resolution of ca. twice the step size given by the scanning step size of 1.3 nm. From these observations, it can be inferred that the blend NPs of PCDTBT and $PC_{71}BM$ exhibit very small compositional demixing, in the size range of ~2 nm, indicating fine mixing at the molecular level. This is in agreement with the optical properties of the blend particles, where effective fluorescence quenching was observed, even for the lowest $PC_{71}BM$ concentration, as a result of fine mixing.

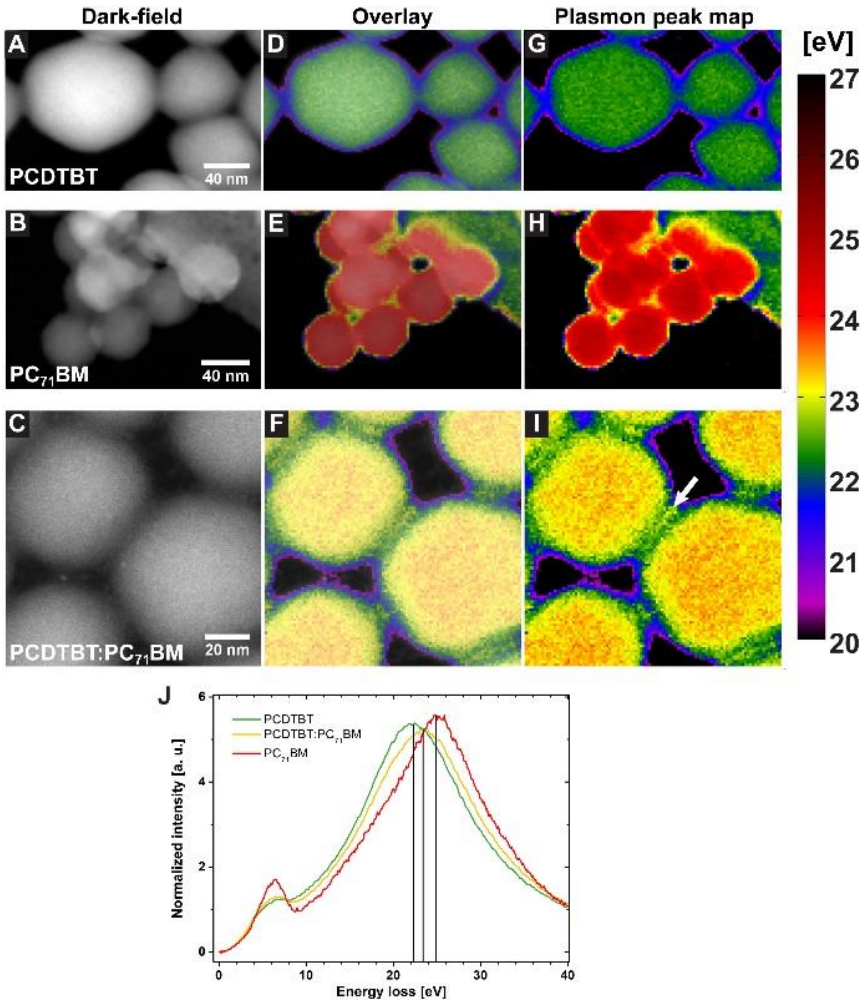

Figure 4. Spectroscopic imaging of different NPs. A-C: STEM dark-field images from **(A)** NP1-0% $PC_{71}BM$, **(B)** NP8-100% $PC_{71}BM$, and blend particles **(C)** NP7-75% $PC_{71}BM$. D-F, G-I: Overlays of dark-field images with plasmon peak maps **(D-F)** and plasmon peak maps **(G-I)** created from Lorentzian fits to spatially resolved plasmon peaks (2 nm step size for pure particles and 1.3 nm step size for blend). The white arrow in (I) points to a small spatial feature, where also mixed PCDTBT and $PC_{71}BM$ is found between joining particles. **(J)** Average low energy-loss spectra from the three samples.

3.4 Device fabrication and characteristics

In order to provide proof-of-principle of the suitability of the proposed NPs for water-solvent prepared solar cells, PCDTBT:$PC_{71}BM$ OPV devices were fabricated out of the PCDTBT:$PC_{71}BM$ (400 wt% $PC_{71}BM$; 1:4) blend NPs, using a glass/ITO/ZnO/PCDTBT:$PC_{71}BM$ NP/MoO_3/Al inverted device architecture, and the nanomorphology of the active layer was studied. The active layer was deposited by spincoating the NP dispersion. The AFM image of the spincoated NPs before annealing (Figure 5A) shows that with spincoating a completely covered NP layer over a large area can be obtained. The AFM image of the annealed device is given in Figure S3 (supporting information). A range of annealing conditions between 140 and 200 °C for the nanoparticle layer were tested. It was found that annealing for 4 minutes at 140 °C resulted in non-working devices, whereas treatment at 200 °C yielded low PCE values (average PCE<0.5%). However, annealing at 160 °C (4 min) and 180°C (4 min) resulted in a best PCE of 1.9% with respectively an average PCE of 1.3±0.4% (Figure S4, supporting information) and 1.4±0.4 %. The current density vs. voltage (*J-V*) curve is provided in Figure 5B for the most efficient PCDTBT:$PC_{71}BM$ OPV device, obtained

after annealing at 180 °C for 4 min, reaching a PCE for the best device of 1.9% (V_{oc} = 570 mV, J_{sc} = 8.69 mA/cm², FF = 38%) and with an average PCE of 1.4±0.4 % (under AM1.5 illumination). To allow proper comparison, reference polymer solar cells were made by spincoating the active layer materials from *o*-DCB solution and employing the same device architecture as the NP based devices. All tested conditions and average PCEs are summarized in the supporting information, Table S2. The reference cell without annealing (Sample - Ref 1, Table S2, supporting information) resulted in a best PCE of 3.7% (average PCE 3.3±0.3%). These values fall below the average efficiencies reported for PCDTBT:$PC_{71}BM$ (5 to 6%) [64,65], which already suggests a negative influence of the ZnO layer on J_{sc} and FF. To take into account the effect that thermal treatment might have on the active layer, annealed reference devices were also studied (Samples - Ref 2 and 3, Table S2, supporting information). Annealing the active layer at 160 °C (4 min) resulted in a decrease of the best PCE to 2% (average 1.6±0.5%), mainly due to a decrease in V_{oc} and FF. Similar effects have also been reported by Gusain et al.[66] This also possibly explains the low V_{oc} and FF in the NP device. Annealing reference devices at 180 °C (4 min) showed similar results, with a PCE for the best device of 2% (average 1.6±0.3%). Additionally, looking at the *J-V* curves in the dark and under light (Figure S5, supporting information), it can be seen that the leakage current is quite high for the NP cell, which may be due to the non-optimal coverage of the annealed NP layer, and can also explain its low V_{oc} and FF. These results indicate that further optimization of the ZnO as well as the photoactive layers and annealing conditions are needed to achieve better efficiencies for the NP devices and that there is still room for improvement. A dark-field STEM image (Figure 5C) of a cross-section obtained by focused ion beam milling reveals the integrity of the different layers of that particular device (in Figure 5B). The active layer thickness varies from about 60 to 80 nm. Figure 5D and 5E show dark-field images and the corresponding plasmon peak map of a part of the photoactive layer, respectively. Again, very small phase separation is observed and could only be visualized by smoothing the map with a Gaussian filter and by adjusting the color map to show only a very small energy range due to the large amount of $PC_{71}BM$ in comparison to the blend NPs studied in Figure 4. Several $PC_{71}BM$ enrichments can be identified after this data treatment. However, the lack of clear demixing, even after annealing, confirms the observation of fine intermixing as observed in the NP state. A region with a slightly thicker photoactive layer of the otherwise homogeneous film was evaluated as well and the data are presented in Figure S6 (supporting information). Irrespective of the small variations in thickness, a similar nanomorphology prevailed, thereby underpinning the overall homogeneity of the film morphology. It could be possible that a homogenization took place during preparation, but we expect no influence on the nanoscale structure due to the focused ion beam milling. It was recently shown that gentle thinning by low-energy ions—as we applied also for this work—preserves the electronic structure [59,67] and can even preserve organic crystallites [68]. For this reason, we expect a reliable image of the morphology in the device cross-section. Furthermore, we performed STEMSI on the nanoparticles that contain 400 wt% $PC_{71}BM$ and that were used to fabricate the best-performing device. A plasmon peak map is provided in Figure S7 (supporting information). Again, only by applying the adapted color map after gentle Gaussian smoothing domains of strong fullerene enrichment can be observed. However, these domains are present with intermittent regions of lower enrichment, no phase separation with PCDTBT. In fact, the morphology of the nanoparticles on the TEM grid is very similar to the structure in the functional device after annealing, which indicates that annealing is required to induce fusion of the particles but does not cause further coarsening or phase separation. The large similarity between nanoparticles and the device photoactive layer made by these nanoparticles also supports the FIB milling did not induce damage to the nanoscale structure.

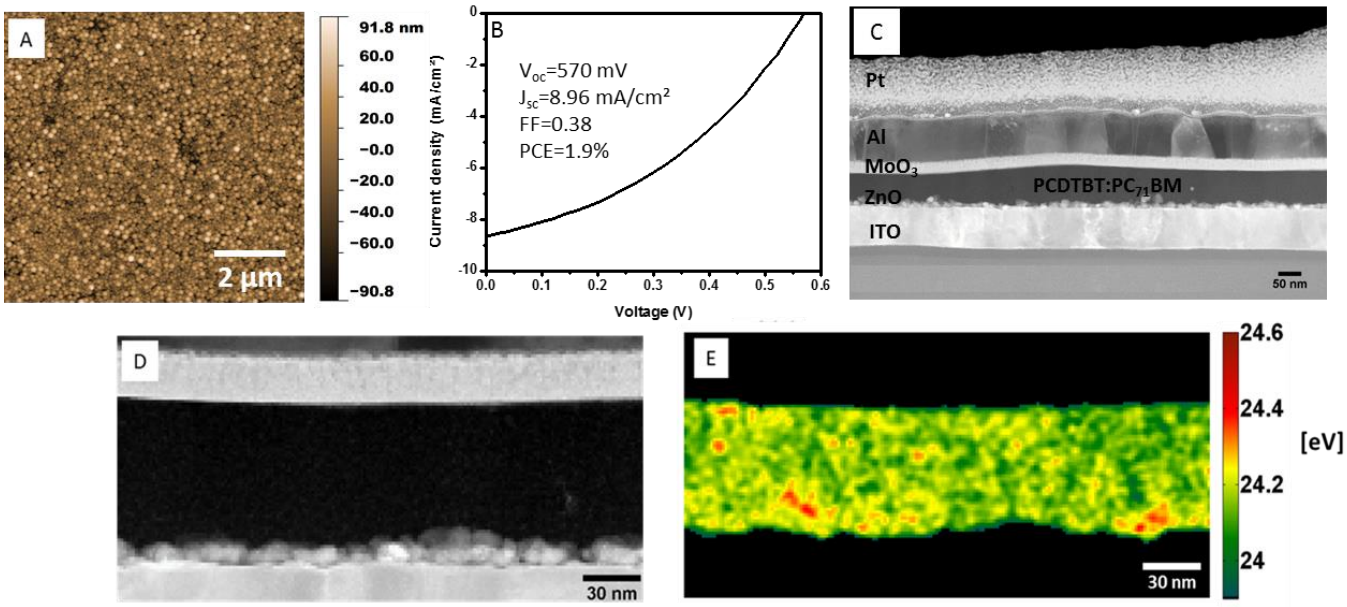

Figure 5. (A) AFM image of spincoated NPs, **(B)** *J-V* curve, **(C)** device assembly, **(D)** dark field overview of the active layer, and **(E)** plasmon peak map of the active layer of a PCDTBT:$PC_{71}BM$ (400 wt% $PC_{71}BM$; 1:4) NP OPV device.

4. CONCLUSIONS

Aqueous dispersions of push-pull polymer PCDTBT:$PC_{71}BM$ blend NPs, employing a high boiling solvent (*o*-DCB) and a high molecular weight polymer, were successfully synthesized by adapting the combined miniemulsion/solvent evaporation technique[29,55]. The blend composition was systematically varied to show the versatility of the technique that can be easily extended for any donor:acceptor combination requiring high boiling solvents. The fluorescence decay studies clearly reveal the effect of mixing and associated quenching of PCDTBT by $PC_{71}BM$, where a loading of 1 Wt% $PC_{71}BM$ already leads to a substantial decrease of $<\tau>$ for the NPs. Concomitantly, the decay trend confirms that the stoichiometry of the NPs can be controlled in a very systematic way during the synthesis. The optical properties signify that the mixing of the constituents and the resulting interface between the two blend materials play a pivotal role in defining the final characteristics of the photoactive layer. The nanomorphology of the blend was studied for the first time at the single NP level using high resolution STEM spectral imaging by mapping the plasmon peaks of the constituents. The results clearly illustrate that blend NPs of PCDTBT and $PC_{71}BM$ exhibit very small compositional demixing, in the size range of ~2 nm, indicating fine mixing at the molecular level.

As a proof-of principle, the aqueous dispersions were used for the fabrication of an eco-friendly polymer solar cell. The device characteristics show promising results, with a PCE of 1.9% for the best device and with an average PCE of 1.4±0.4 %. With further optimization of the photoactive layer (annealing conditions and layer thickness), higher PCE values are expected and currently optimization of the layer using different deposition techniques is in progress. The nanomorphology of the photoactive layer from the device structure obtained by cross-section STEM analysis reflects the morphology observed for the individual NPs. This observation is highly intriguing as these NPs can be regarded as analogous systems to active layer films in a device, offering the functionality of bulk materials but without significant interparticle heterogeneity[26,27,28]. Therefore, apart from offering eco-friendly large scale processing of organic solar cells, these particles are also interesting for studying the structure-property-performance of active layer materials.

It is also important to emphasize that the particle synthesis adopted here can be easily extended for testing new and existing push-pull polymers requiring environmentally unfavourable high boiling solvents. As an additional outlook, it will certainly stimulate the research interest of many groups developing advanced chemical structures for improved PCEs to validate their materials for aqueous processing of devices.

APPENDICES

Appendix A

Supporting Information: UV-Vis spectra, TEM defocus series, AFM, solar cell characteristics and cross sectional TEM

AUTHOR INFORMATION

Corresponding Author

*Anitha Ethirajan: anitha.ethirajan@uhasselt.be

Author Contributions

L.D. performed the synthesis and the characterization of all nanoparticles. L.D. also made the solar cells and the device characterizations. M.P. did all the TEM characterizations. E.F. performed the optical spectroscopy measurements. I.C. made the AFM characterizations. M.V. helped with the data interpretation of the optical spectroscopy part. G.V. and S.B. contributed to the data interpretation related to TEM measurements. W.M., D.V., and J.M. were involved in the scientific discussions. A.E. conceived the research and planned the experiments. All authors contributed in writing the manuscript.

ACKNOWLEDGMENT

This work was supported by BOF funding of Hasselt University, the Interreg project Organext, and the IAP 7/05 project FS2 (Functional Supramolecular Systems), granted by the Science Policy Office of the Belgian Federal Government (BELSPO). A.E. is a post-doctoral fellow of the Flanders Research Foundation (FWO). M.P. gratefully acknowledges the SIM NanoForce program for financial support. S.B. further acknowledges financial support from the European Research Council (ERC Starting Grant #335078-COLOURATOMS). The authors are thankful for technical support by J. Smits, T. Vangerven, and J. Baccus.

REFERENCES

[1] K. A. Mazzio and C. K. Luscombe, The future of organic photovoltaics. Chem. Soc. Rev. 44 (2015) 78-90.

[2] S. Lizin, S. Van Passel, E. De Schepper, W. Maes, L. Lutsen, J. Manca and D. Vanderzande, Life cycle analyses of organic photovoltaics: a review. Energy Environ. Sci. 6 (2013) 3136-3149.

[3] C. H. Peters, I. T. Sachs-Quintana, J. P. Kastrop, S. Beaupré, M. Leclerc and M. D. McGehee, High efficiency polymer solar cells with long operating lifetimes. Adv. Energy Mater. 1 (2011) 491-494.

[4] W. R. Mateker, I. T. Sachs-Quintana, G. F. Burkhard, R. Cheacharoen and M. D. McGehee, Minimal long-term intrinsic degradation observed in a polymer solar cell illuminated in an oxygen-free environment. Chem. Mater. 27 (2015) 404-407.

[5] E. Bundgaard and F. C. Krebs, Low band gap polymers for organic photovoltaics. Sol. Energ. Mat. Sol. C. 91 (2007) 954-985.

[6] C. Liu, K. Wang, X. Gong and A. J. Heeger, Low bandgap semiconducting polymers for polymeric photovoltaics. Chem. Soc. Rev. (2016) DOI: 10.1039/c5cs00650c

[7] J. W. Kingsley, P. P. Marchisio, H. Yi, A. Iraqi, C. J. Kinane, S. Langridge, R. L. Thompson, A. J. Cadby, A. J. Pearson, D. G. Lidzey, R. A. L. Jones and A. J. Parnell, Molecular weight dependent vertical composition profiles of PCDTBT:$PC_{71}BM$ blends for organic photovoltaics. Sci. Rep. 4 (2014) 5286.

[8] Y. Zhang, E. Bovill, J. Kingsley, A. R. Buckley, H. Yi, A. Iraqi, T. Wang and D. G. Lidzey, PCDTBT based solar cells: one year of operation under real-world conditions. Sci. Rep. 6 (2016) 21632.

[9] S. H. Park, A. Roy, S. Beaupré, S. Cho, N. Coates, J. S. Moon, D. Moses, M. Leclerc, K. Lee and A. J. Heeger, Bulk heterojunction organic solar cells with internal quantum efficiency approaching 100%. Nat. Photonics 3 (2009) 297-302.

[10] Y. Liu, J. Zhao, Z. Li, C. Mu, W. Ma, H. Hu, K. Jiang, H. Lin, H. Ade and H. Yan, Aggregation and morphology control enables multiple cases of high-efficiency polymer solar cells. Nat Commun. 5 (2014) 5293.

[11] M. C. Scharber, On the efficiency limit of conjugated polymer:fullerene-based bulk heterojunction organic solar cells. Adv. Mater. 28 (2016) 1994–2001.

[12] G. Pirotte, J. Kesters, P. Verstappen, S. Govaerts, J. Manca, L. Lutsen, D. Vanderzande and W. Maes, Continuous flow polymer synthesis toward reproducible large-scale production for efficient bulk heterojunction organic solar cells. ChemSusChem 8 (2015) 3228-3233.

[13] F. C. Krebs, Fabrication and processing of polymer solar cells: A review of printing and coating techniques. Sol. Energ. Mat. Sol. C. 93 (2009) 394-412.

[14] C. Sprau, F. Buss, M. Wagner, D. Landerer, M. Koppitz, A. Schulz, D. Bahro, W. Schabel, P. Scharfer and A. Colsmann, Highly efficient polymer solar cells cast from non-halogenated xylene/anisaldehyde solution. Energy Environ. Sci. 8 (2015) 2744-2752.

[15] S. Zhang, L. Ye, H. Zhang and J. Hou, Green-solvent-processable organic solar cells. Mater. Today (2016) http://dx.doi.org/10.1016/j.mattod.2016.02.019.

[16] S. Li, H. Zang, W. Zhao, L. Ye, H. Yao, B. Yang, S. Zhang, J. Hou, Green-Solvent-Processed All-Polymer Solar Cells Containing a Perylene Diimide-Based Acceptor with an Efficiency over 6.5%. Adv. Energy Mater. 6 (2016) 1501991.

[17] Yulia Galagan and Ronn Andriessen (2012). Organic Photovoltaics: Technologies and Manufacturing, Third Generation Photovoltaics, Dr. Vasilis Fthenakis (Ed.), ISBN: 978-953-51-0304-2, InTech, Available from: http://www.intechopen.com/books/third-generation-photovoltaics/organic-photovoltaics-technologies-andmanufacturing.

[18] D. Darwis, N. Holmes, D. Elkington, A. L. David Kilcoyne, G. Bryant, X. Zhou, P. Dastoor and W. Belcher, Surfactant-free nanoparticulate organic photovoltaics. Sol. Energ. Mat. Sol. C. 121 (2014) 99-107.

[19] N. P. Holmes, K. B. Burke, P. Sista, M. Barr, H. D. Magurudeniya, M. C. Stefan, A. L. D. Kilcoyne, X. Zhou, P. Dastoor and W. J. Belcher, Nano-domain behaviour in P3HT:PCBM nanoparticles, relating material properties to morphological changes. Sol. Energ. Mat. Sol. C., 117 (2013) 437-445.

[20] K. B. Burke, A. J. Stapleton, B. Vaughan, X. Zhou, A. L. D. Kilcoyne, W. Belcher and P. Dastoor, Scanning transmission x-ray microscopy of polymer nanoparticles: probing morphology on sub-10nm length scales. Nanotechnology 22 (2011) 265710.

[21] A. Stapleton, B. Vaughan, B. Xue, E. Sesa, K. Burke, X. Zhou, G. Bryant, O. Werzer, A. Nelson, A. L. David Kilcoyne, L. Thomsen, E. Wanless, W. Belcher and P. Dastoor, A multilayer approach to polyfluorene water-based organic photovoltaics. Sol. Energ. Mat. Sol. C. 102 (2012) 114-124.

[22] S. Ulum, N. Holmes, M. Barr, A. L. D. Kilcoyne, B. B. Gong, X. Zhou, W. Belcher and P. Dastoor, The role of miscibility in polymer:fullerene nanoparticulate organic photovoltaic devices. Nano Energy 2 (2013) 897-905.

[23] S. Ulum, N. Holmes, D. Darwis, K. Burke, A. L. David Kilcoyne, X. Zhou, W. Belcher and P. Dastoor, Determining the structural motif of P3HT:PCBM nanoparticulate organic photovoltaic devices. Sol. Energ. Mat. Sol. C. 110 (2013) 43-48.

[24] B. Vaughan, E. Williams, N. Holmes, S. Prashant, A. Dodabalapur, P. Dastoor and W. Belcher, Water-based nanoparticulate solar cells using a diketopyrrolopyrrole donor polymer. Phys. Chem. Chem. Phys. 16 (2014) 2647-2653.

[25] S. Gärtner, M. Christmann, S. Sankaran, H. Röhm, E.-M. Prinz, F. Penth, A. Pütz, A. E. Türeli, B. Penth, B. Baumstümmler and A. Colsmann, Eco-friendly fabrication of 4% efficient organic solar cells from surfactant-free P3HT:ICBA nanoparticle dispersions. Adv. Mater. 26 (2014) 6653-6657.

[26] Z. Hu and A. J. Gesquiere, PCBM concentration dependent morphology of P3HT in composite P3HT/PCBM nanoparticles. Chem. Phys. Lett. 476 (2009) 51-55.

[27] Z. Hu, D. Tenery, M. S. Bonner and A. J. Gesquiere, Correlation between spectroscopic and morphological properties of composite P3HT/PCBM nanoparticles studied by single particle spectroscopy. J. Lumin. 130 (2010) 771-780.

[28] D. Tenery, J. G. Worden, Z. Hu and A. J. Gesquiere, Single particle spectroscopy on composite MEH-PPV/PCBM nanoparticles. J. Lumin. 129 (2009) 423-429.

[29] T. Kietzke, D. Neher, K. Landfester, R. Montenegro, R. Guntner and U. Scherf, Novel approaches to polymer blends based on polymer nanoparticles. Nat. Mater. 2 (2003) 408-412.

[30] S. Sankaran, K. Glaser, S. Gärtner, T. Rödlmeier, K. Sudau, G. Hernandez-Sosa and A. Colsmann, Fabrication of polymer solar cells from organic nanoparticle dispersions by doctor blading or ink-jet printing. Org. Electron. 28 (2016) 118-122.

[31] N. P. Holmes, M. Marks, P. Kumar, R. Kroon, M. G. Barr, N. Nicolaidis, K. Feron, A. Pivrikas, A. Fahy, A. D. d. Z. Mendaza, A. L. D. Kilcoyne, C. Müller, X. Zhou, M. R. Andersson, P. Dastoor and W. J. Belcher, Nano-pathways: Bridging the divide between water-processable nanoparticulate and bulk heterojunction organic photovoltaics. Nano Energy 19 (2016) 495-510.

[32] T. R. Andersen, T. T. Larsen-Olsen, B. Andreasen, A. P. L. Böttiger, J. E. Carlé, M. Helgesen, E. Bundgaard, K. Norrman, J. W. Andreasen, M. Jørgensen and F. C. Krebs, Aqueous processing of low-band-gap polymer solar cells using roll-to-roll methods. ACS Nano 5 (2011) 4188-4196.

[33] N. A. D. Yamamoto, M. E. Payne, M. Koehler, A. Facchetti, L. S. Roman and A. C. Arias, Charge transport model for photovoltaic devices based on printed polymer:fullerene nanoparticles. Sol. Energ. Mat. Sol. C 141 (2015) 171-177.

[34] J. S. Moon, J. Jo and A. J. Heeger, Nanomorphology of PCDTBT:$PC_{70}BM$ bulk heterojunction solar cells. Adv. Energy Mater. 2 (2012) 304-308.

[35] Z. M. Beiley, E. T. Hoke, R. Noriega, J. Dacuña, G. F. Burkhard, J. A. Bartelt, A. Salleo, M. F. Toney and M. D. McGehee, Morphology-dependent trap formation in high performance polymer bulk heterojunction solar cells. Adv. Energy Mater. 1 (2011) 954-962.

[36] N. Banerji, S. Cowan, M. Leclerc, E. Vauthey and A. J. Heeger, Exciton formation, relaxation and decay in PCDTBT. J. Am. Chem. Soc. 132 (2010) 17459-17470.

[37] F. Etzold, I. A. Howard, R. Mauer, M. Meister, T.-D. Kim, K.-S. Lee, N. S. Baek and F. Laquai, Ultrafast exciton dissociation followed by nongeminate charge recombination in PCDTBT:PCBM photovoltaic blends. J. Am. Chem. Soc. 133 (2011) 9469-9479.

[38] M. Tong, N. E. Coates, D. Moses, A. J. Heeger, S. Beaupré and M. Leclerc, Charge carrier photogeneration and decay dynamics in the poly(2,7-carbazole) copolymer PCDTBT and in bulk heterojunction composites with $PC_{70}BM$. Phys. Rev. B 81 (2010) 125210.

[39] G. Fang, J. Liu, Y. Fu, B. Meng, B. Zhang, Z. Xie and L. Wang, Improving the nanoscale morhology and processibility for PCDTBT-based polymer solar cells via solvent mixtures. Org. Electron. 13 (2012) 2733-2740.

[40] N. Boens, W. Qin, N. Basarić, J. Hofkens, M. Aemloot, J. Pouget, J.P. Lefèvre, B. Valeur, E. Gratton, M. Vandeven, N.D. Silva, Y. Engelborghs, K. Willaers, A. Sillen, G. Rumbles, D. Philips, A.J.W.G. Visser, A. van Hoek, J.R. Lakowicz, H. Malak, I. Gryczynski, A.G. Szabo, D.T. Krajcarski, N. Tamai, A. Miura, Fluorescence lifetime standards for time and frequency domain fluorescence spectroscopy. Anal. Chem. 79 (2007) 2137-2149.

[41] T. Wang, A. J. Pearson, A. D. F. Dunbar, P. A. Staniec, D. C. Watters, H. Yi, A. J. Ryan, R. A. L. Jones, A. Iraqi and D. G. Lidzey, Correlating structure with function in thermally annealed PCDTBT:$PC_{70}BM$ photovoltaic blends. Adv. Funct. Mater. 22 (2012) 1399-1408.

[42] S. Alem, T.-Y. Chu, S. C. Tse, S. Wakim, J. Lu, R. Movileanu, Y. Tao, F. Bélanger, D. Désilets, S. Beaupré, M. Leclerc, S. Rodman, D. Waller and R. Gaudiana, Effect of mixed solvents on PCDTBT:$PC_{70}BM$ based solar cells. Org. Electron. 12 (2011) 1788-1793.

[43] H. Kang, M. A. Uddin, C. Lee, K.-H. Kim, T. L. Nguyen, W. Lee, Y. Li, C. Wang, H. Y. Woo and B. J. Kim, Determining the role of polymer molecular weight for high-performance all-polymer solar cells: its effect on polymer aggregation and phase separation. J. Am. Chem. Soc. 137 (2015) 2359-2365.

[44] T. Vangerven, P. Verstappen, J. Drijkoningen, W. Dierckx, S. Himmelberger, A. Salleo, D. Vanderzande, W. Maes and J. V. Manca, Molar mass versus polymer solar cell performance: highlighting the role of homocouplings. Chem. Mater. 27 (2015) 3726-3732.

[45] T. Kietzke, D. Neher, M. Kumke, O. Ghazy, U. Ziener and K. Landfester, Phase separation of binary blends in polymer nanoparticles. Small 3 (2007) 1041-1048.

[46] R. H. Staff, D. Schaeffel, A. Turshatov, D. Donadio, H.-J. Butt, K. Landfester, K. Koynov and D. Crespy, Particle formation in the emulsion-solvent evaporation process. Small 9 (2013) 3514-3522.

[47] N. Blouin, A. Michaud and M. Leclerc, A low-bandgap poly(2,7-carbazole) derivative for use in high-performance solar cells. Adv. Mater. 19 (2007) 2295-2300.

[48] Y. Huang, E. J. Kramer, A. J. Heeger and G. C. Bazan, Bulk heterojunction solar cells: morphology and performance relationships. Chem. Rev. 114 (2014) 7006–7043.

[49] M. Pfannmöller, W. Kowalsky and R. R. Schröder, Visualizing physical, electronic, and optical properties of organic photovoltaic cells. Energy Environ. Sci. 6 (2013) 2871-2891.

[50] M. Maus, E. Rousseau, M. Cotlet, G. Schweitzer, J. Hofkens, M. Van der Auweraer, F. C. De Schryver and A. Krueger, New picosecond laser system for easy tunability over the whole ultraviolet/visible/near infrared wavelength range based on flexible harmonic generation and optical parametric oscillation. Rev. Sci. Instrum. 72 (2001) 36-40.

[51] R. F. Egerton and M. Takeuchi, Radiation damage to fullerite (C_{60}) in the transmission electron microscope. Appl. Phys. Lett. 75 (1999) 1884-1886.

[52] R. F. Egerton, Electron energy-loss spectroscopy in the electron microscope, Springer, 1996.

[53] D. W. Johnson and J. C. H. Spence, Determination of the single-scattering probability distribution from plural-scattering data. J. Phys. D: Appl. Phys 7 (1974) 771.

[54] J. Kesters, T. Ghoos, H. Penxten, J. Drijkoningen, T. Vangerven, D. M. Lyons, B. Verreet, T. Aernouts, L. Lutsen, D. Vanderzande, J. Manca and W. Maes, Imidazolium-substituted polythiophenes as efficient electron transport materials improving photovoltaic performance. Adv. Energy Mater. 3 (2013) 1180-1185.

[55] K. Landfester, Miniemulsion polymerization and the structure of polymer and hybrid nanoparticles. Angew. Chem. Int. Ed. 48 (2009) 4488-4507.

[56] S. N. Clafton, D. M. Huang, W. R. Massey and T. W. Kee, Femtosecond dynamics of excitons and hole-polarons in composite P3HT/PCBM nanoparticles. J. Phys. Chem. B 117 (2013) 4626-4633.

[57] M. Pfannmöller, H. Flügge, G. Benner, I. Wacker, C. Sommer, M. Hanselmann, S. Schmale, H. Schmidt, F. A. Hamprecht, T. Rabe, W. Kowalsky and R. R. Schröder, Visualizing a homogeneous blend in bulk heterojunction polymer solar cells by analytical electron microscopy. Nano Lett. 11 (2011) 3099-3107.

[58] S. Albrecht, S. Janietz, W. Schindler, J. Frisch, J. Kurpiers, J. Kniepert, S. Inal, P. Pingel, K. Fostiropoulos, N. Koch and D. Neher, Fluorinated copolymer PCDTBT with enhanced open-circuit voltage and reduced recombination for highly efficient polymer solar cells. J. Am. Chem. Soc. 134 (2012) 14932-14944.

[59] M. Pfannmöller, H. Heidari, L. Nanson, O. R. Lozman, M. Chrapa, T. Offermans, G. Nisato and S. Bals, Quantitative tomography of organic photovoltaic blends at the nanoscale. Nano Lett. 15 (2015) 6634-6642.

[60] D. M. DeLongchamp, R. J. Kline and A. Herzing, Nanoscale structure measurements for polymer-fullerene photovoltaics. Energy Environ. Sci. 5 (2012) 5980-5993.

[61] M. Pfannmöller, H. Flügge, G. Benner, I. Wacker, W. Kowalsky and R. R. Schröder, Visualizing photovoltaic nanostructures with high-resolution analytical electron microscopy reveals material phases in bulk heterojunctions. Synt. Met. 161 (2012) 2526-2533.

[62] W. Schindler, M. Wollgarten and K Fostiropoulos, Revealing nanoscale phase separation in small-molecule photovoltaic blends by plasmonic contrast in the TEM. Org. Electron. 13 (2012) 1100-1104.

[63] S. B. Dkhil, M. Pfannmöller, S. Bals, T. Koganezawa, N. Yoshimoto, D. Hannani, M. Gaceur, C. Videlot-Ackermann, O. Margeat, J. Ackermann, Square-Centimeter-Sized High-Efficiency Polymer Solar cells: How the Processing Atmosphere and Film Quality Influence Performance at Large Scale. Adv. Energy. Mater. 6 (2016) doi: 10.1002/aenm.201600290.

[64] Y. Sun, J. Seo, C.J. Takacs, J. Steifter, A.J. Heeger, Inverted polymer solar cells integrated with a low-temperature-annealed sol-gel-derived ZnO film as an electron transport layer. Adv. Mater. 23 (2011) 1679-1683.

[65] E. Voroshazi, I. Cardinaletti, T. Conard, B.P. Rand, Light-induced degradation of polymer:fullerene photovoltaic devices: an intrinsic or material-dependent failure mechanism? Adv. Energy Mater. 4 (2014) 1614-6840.

[66] A. Gusain, V. Saxena, P. Veerender, P. Jha, S. P. Koiry, A.K. Chauhan, D.K. Aswal, S.K. Gupta, Investigation on the Effects of Thermal Annealing on PCDTBT:PCBM Bulk-Heterojunction Polymer Solar Cells. AIP Conf. Proc. 1512 (2013) 776-777.

[67] A. Guerrero, M. Pfannmöller, A. Kovalenko, T. S. Ripolles, H. Heidari, S. Bals, L. Kaufmann, J. Bisquert, G. Garcia-Belmonte, Nanoscale mapping by electron energy-loss spectroscopy reveals evolution of organic solar cell contact selectivity. Org. electron. 16 (2015) 227-233.

[68] J. B. Gilchrist, T. H. Basey-Fisher, S. Chang, F. Scheltens, D. W. McComb, S. Heutz, Uncovering Buried Structure and Interfaces in Molecular Photovoltaics. Adv. Function. Mater. 24 (2014) 6473-6483.